Supplementary Data

Alexeeva et al. 2018 *10.1093/nar/gky1184*

Comment on β-elimination products produced by EcNth and hOGG1

Our preparation of the samples for PAGE at room temperature, instead of at the complete denaturing conditions at 95 °C, caused no difference in electrophoretic mobility between the 5′-incision fragments formed by EcFpg and EcNfo/hAPE1 (Figures 3A and 7). In contrast, for EcNth the conventional 95 °C-treatment resulted in one major band defining the 3′-dRP (Figure 3A) whereas the room temperature treatment resulted in two bands corresponding to both the 3′-dRP and the 3′-α,β-unsaturated aldehyde ends (Figure 7). For hOGG1 we observed the same bands although the 3′-α,β-unsaturated aldehyde tended to be the major product (data not shown). This accords with previous results indicating that hOGG1 (1,2) as well as EcNth (3) form two to several β-elimination products. EcNth and hOGG1 incise AP sites by a β-elimination reaction resulting in similar enzyme-substrate intermediates (3-10). However, the atomic site of subsequent water addition and/or whether one or two water molecules are added may determine whether the result is a 3′-dRP or a 3′-α,β-unsaturated aldehyde (11). Spontaneous interchange (dehydration/hydration) between the two forms may also complicate interpretation of results.

A three-phase kinetic model

Theoretical and experimental arguments for a three-phase model

We developed a model describing the hSMUG1 (E) kinetics of uracil excision and U-DNA incision in three phases/stages (Figure 9A), which corresponds well with the experimental data (Figures 9B, 9C and S5).

Phase 1: Rapid uracil excision. In the first stage, E binds DNA_U and rapidly releases U to form DNA_{AP}. As a simplification, we avoid considering a reversible binding between DNA and E, which leads to the overall excision reaction

$$E + DNA_U \xrightarrow{k_1} DNA_{AP} \cdot U \cdot E \xrightarrow{k_p^{ex}} DNA_{AP} + U + E \qquad (1)$$

To determine the rate constants k_1 and k_p^{ex} we used an initial U-DNA concentration [DNA_U] of 50 mM and adjusted the constants to the best "eye-balled" fit (see Figure 9C). The values of k_1 (1.5 nM^{-1} min^{-1}) and k_p^{ex} obtained were kept in later calculations with more processes added to the model and at higher initial [DNA_U]. The velocity V^{ex} is calculated as [DNA_{AP}] (which equals [U] released) divided by the 20 min assay time, *i.e.*

$$V^{ex} = [DNA_{AP}]/20 \text{ (nM/min)} \qquad (2)$$

Note that the 2.5 nM/min-level in Figure 9C does not result from enzyme saturation, but reflects that all of the 50 nM DNA_U is processed within the 20 min assay time resulting in the maximal V^{ex}. The excision reaction is relatively rapid, indicating that an [E] of 0.2 nM processes all initial DNA within 20 min.

Phase 2: Slow adsorption/desorption of enzyme to DNA. Reaction (1) shows that DNA_{AP} forms together with (free) U. The model assumes that E binds and dissociates randomly and non-specifically at different places on DNA_{AP}. At low [E], few E molecules are adsorbed on the DNA_{AP} surface, while at higher [E], the DNA_{AP} is more densely populated by E which continuously adsorbs and desorbs (Figure 9A). Whenever E binds at the AP or cleavage site DNA_{AP} cleaves into P1 and P2. The kinetics of the enzyme adsorption/desorption process can be described as

$$E + DNA_{AP,\, j\neq i} \underset{k_{-1}}{\overset{k_1}{\rightleftharpoons}} E \cdot DNA_{AP,\, j\neq i} \qquad (3)$$

where *j* is any site on DNA except the incision site *i*. If we assume that a single DNA_{AP} molecule has *N* unspecific binding sites for E, with n_{empty} describing the number of sites without E, while n_{occ} describes the sites on DNA_{AP} occupied by E, it gives

$$n_{occ} + n_{empty} = N \qquad (4)$$

The rate of adsorption is dependent on the number of vacant sites, n_{empty}, and the concentration of E in the solution, *i.e.*

$$V^{adsorp} = k_1 \cdot n_{empty} \cdot [E] \qquad (5)$$

The rate of desorption, in contrast, is determined by the number of E-occupied sites only, *i.e.*

$$V^{desorp} = k_{-1} \cdot n_{occ} \qquad (6)$$

At steady state/dynamical equilibrium

$$V^{adsorp} = V^{desorp} \qquad (7)$$

Using Θ instead of n_{occ} we write at steady state

$$k_{-1} \cdot \Theta_{ss} = k_1 \cdot (N - \Theta_{ss})\,[E] \qquad (8)$$

which solved for Θ_{ss} gives

$$\Theta_{ss} = k_1 \cdot N \cdot [E]/(k_{-1} + k_1 \cdot [E]) = N \cdot [E]/(K_D + [E]) \text{ where } K_D = k_1/k_{-1} \qquad (9)$$

and shows that the number of E-occupied sites follows a saturation curve in [E], also called an *adsorption isotherm* (12).

Since E only bound to the AP or incision site *i* leads to cleavage of DNA_{AP},

$$E + DNA_{AP,\,i} \rightleftharpoons E \cdot DNA_{AP,\,i} \xrightarrow{k_1^{in}} E + P1 + P2 \qquad (10)$$

it is needed to calculate the probability that E binds at site *i*. The simplest assumption is that the binding probability $\mathcal{P}$ is equal for the *N* sites. In that case, the probability $\mathcal{P}$ that E binds at the site *i* for a single DNA_{AP} molecule (or one mole DNA_{AP}) is

$$\mathcal{P} = \Theta_{ss}/N = [E]/(K_D + [E]) \qquad (11)$$

Thus, the reaction rate for cleaving DNA_{AP} to form P1, while E is still adsorbing at empty binding sites on DNA_{AP}, is

$$V^{in} = V_1^{in} = k_1^{in} \cdot [DNA_{AP}]\,([E]/(K_D + [E])) \qquad (12)$$

Equation (12) describes the rate of formation of the measured product P1 during the adsorption/desorption phase 2 (Figure 9A).

Phase 3: Slow incision of AP site. With increasing initial [E], E eventually occupies all binding sites on DNA_{AP}, *i.e.*, DNA_{AP} is saturated with adsorbed E and no more E will bind. However, at the AP site, E cleaves DNA and the rate of cleavage is (approximately) proportional to $[DNA_{AP} \cdot E]$ (the latter denotes the concentration of DNA_{AP} saturated with adsorbed E molecules; Figure 9A), giving

$$E + DNA_{AP} \xrightarrow{k_2} DNA_{AP} \cdot E \xrightarrow{k_2^{in}} P1 + P2 + E \qquad (13)$$

where k_2 was determined as 0.002 $nM^{-1}\,min^{-1}$. To simplify, we have neglected the non-reactive dissociation of $DNA_{AP} \cdot E$ back to E and DNA_{AP}, as formulated in Equation (10).

Considering the first step as irreversible, the cleavage rate of DNA_{AP} to produce P1 under saturating conditions of E is

$$V_2^{in} = k_2^{in} \cdot [DNA_{AP} \cdot E] \qquad (14)$$

Overview of the kinetic model

The model describes the hSMUG1 (E) excision/incision kinetics during three phases/stages (Figure 9A). First, a rapid initial uracil excision phase 1 occurs and converts the U site into an AP site resulting in $DNA_U \rightarrow DNA_{AP}$. A less reactive phase 2 follows when E binds non-specifically at different sites including the AP site. When bound to the AP site E induces cleavage of DNA_{AP}, which leads to the products P1 and P2 and the release of E. In the final phase 3, high [E] saturates DNA_{AP} because E binds at the non-reactive sites forming a dynamic equilibrium (steady state). Further changes in [E] are only affecting the rate of cleavage when E binds to the AP site.

The following set of reactions/equations describes the model:

$$E + DNA_U \xrightarrow{k_1} DNA_{AP} \cdot U \cdot E \xrightarrow{k_p^{ex}} DNA_{AP} + U + E \qquad (1)$$

$$DNA_{AP} \xrightarrow[k_1^{in},\, K_D]{E} P1 + P2 \qquad (15)$$

with $$V_1^{in} = k_1^{in} \cdot [DNA_{AP}] \cdot ([E]/(K_D + [E])) \qquad (16)$$

and $$E + DNA_{AP} \xrightarrow{k_2} DNA_{AP} \cdot E \xrightarrow{k_2^{in}} P1 + P2 + E \qquad (13)$$

The total formation rate of P1 (the measured product UIP) is

$$\left(\frac{d[P1]}{dt}\right)_{total} = \overbrace{k_1^{in} \cdot [DNA_{AP}] \cdot ([E]/(K_D + [E]))}^{V_1^{in}\text{(competition with unspecific binding sites)}} + \overbrace{k_2^{in} \cdot [DNA_{AP} \cdot E]}^{V_2^{in}\text{(E saturated at unspecific binding sites)}} \qquad (17)$$

The excision rate of uracil is

$$\frac{d[U]}{dt} = k_p^{ex} \cdot [DNA_{AP} \cdot U \cdot E] \qquad (18)$$

The other rate equations are:

$$\frac{d[\mathrm{E}]}{dt} = -\mathrm{k}_1\,[\mathrm{E}]\cdot\left[\mathrm{DNA_U}\right] + \mathrm{k_p^{ex}}[\mathrm{DNA_{AP}}\cdot\mathrm{U}\cdot\mathrm{E}] - \mathrm{k}_2\,[\mathrm{E}]\cdot\left[\mathrm{DNA_{AP}}\right] + \mathrm{k_2^{in}}[\mathrm{DNA_{AP}}\cdot\mathrm{E}] \qquad (19)$$

$$\frac{d\left[\mathrm{DNA_U}\right]}{dt} = -\mathrm{k}_1\,[\mathrm{E}]\cdot\left[\mathrm{DNA_U}\right] \qquad (20)$$

$$\frac{d\left[\mathrm{DNA_{AP}}\cdot\mathrm{U}\cdot\mathrm{E}\right]}{dt} = \mathrm{k}_1\,[\mathrm{E}]\cdot\left[\mathrm{DNA_U}\right] - \mathrm{k_p^{ex}}[\mathrm{DNA_{AP}}\cdot\mathrm{U}\cdot\mathrm{E}] \qquad (21)$$

$$\frac{d\left[\mathrm{DNA_{AP}}\right]}{dt} = \mathrm{k_p^{ex}}[\mathrm{DNA_{AP}}\cdot\mathrm{U}\cdot\mathrm{E}] - \mathrm{k}_2\,[\mathrm{E}]\cdot\left[\mathrm{DNA_{AP}}\right] - \mathrm{k_1^{in}}[\mathrm{DNA_{AP}}]([\mathrm{E}]/(\mathrm{K_D} + [\mathrm{E}])) \qquad (22)$$

The above (rate) equations were solved numerically by using the Fortran subroutine LSODE as described in Materials and Methods.

Discussion

Figures 9B, 9C and S5 show a relative good agreement between the calculated and measured values, despite the simplicity of the model. The model predicts that with increasing DNA concentration the number of unspecific binding sites increases proportionally to *N times* the concentration of DNA, while the number of cleavable sites increases only proportionally with the concentration of DNA. If we assume that all binding sites have an equal probability to bind E, then the probability to bind at the cleavable site is the inverse of the number of binding sites. Thus, the rate of $\mathrm{DNA_{AP}}$ cleavage with constant E concentration should be inversely proportional to $N \cdot [\mathrm{DNA}]_0$, *i.e.*

$$\mathrm{k_1^{in}} = \frac{\kappa}{N\cdot[\mathrm{DNA}]_0} \qquad (23)$$

where κ is a constant. Thus, $\mathrm{k_1^{in}}$ can be estimated for different initial DNA concentrations once a $\mathrm{k_1^{in}}$ value is assigned to an initial DNA concentration. For example, we now assume that $\mathrm{k_1^{in}}([\mathrm{DNA}]_{0.1})$ denotes $\mathrm{k_1^{in}}$ at an initial DNA concentration of 0.1 nM, while $\mathrm{k_1^{in}}([\mathrm{DNA}]_{0.2})$ denotes $\mathrm{k_1^{in}}$ at an initial DNA concentration of 0.2 nM. If the value of

$k_1^{in}([DNA]_{0.1})$ is known, our assumption that E binds non-specifically with equal probability to the *N* binding sites predicts that $k_1^{in}([DNA]_{0.2})$ can be calculated according to

$$k_1^{in}\left([DNA]_{0.2}\right) = k_1^{in}\left([DNA]_{0.1}\right) \cdot \left(\frac{[DNA]_{0.1}}{[DNA]_{0.2}}\right) \qquad (24)$$

If we take $[DNA]_{0.1}$ = 50 nM with a corresponding $k_1^{in}([DNA]_{0.1})$ = 0.009 min^{-1}, then the k_1^{in} value for 375 nM is calculated as

$$k_1^{in}(375\ nM) = k_1^{in}(50\ nM) \cdot \left(\frac{50}{375}\right) = 0.0012\ min^{-1} \qquad (25)$$

This value of k_1^{in}(375 nM) is the same value as used above for the 375 nM curve fit. We performed the curve-fit adjustment before we realised that increasing DNA values increase the number of unspecific binding sites and actually decrease the probability of DNA cleavage. We believe that this is a relative strong argument for a random-access model, where hSMUG1 binds DNA randomly and not specifically. However, we only consider the model as semi-quantitative, because the experimental results determining reaction rates by gel data have considerable uncertainties.

Production of purified hSMUG1(25–270)

E. coli BL21(DE3) harbouring pETM-11-hSMUG1 which codes for a truncated and His-tagged wild-type protein [hSMUG1(25–270)-(His)×6-tag; consists of the amino acids 25–270], was grown in 400 ml auto-induced media containing kanamycin (50 µg/ml) at 28 °C for 24 h. The following procedures were performed at 4 °C or on ice. Cells were harvested by centrifugation, suspended in 25 ml lysis buffer (50 mM HEPES, pH 8.0, 300 mM NaCl, 5% (v/v) glycerol, 1 mM DTT, 1× Complete EDTA-free protease inhibitor cocktail) and lysed by the addition of 100 µg/ml lysozyme (final concentration) by incubation for 30 min at 4 °C with gentle shaking. The cell lysate was supplemented with 0.5% (v/v) Tergitol, 5 mM $MgCl_2$, 5 µg/ml DNase I and 5 µg/ml RNase A and incubated for an additional 30 min at 4 °C

with gentle shaking followed by centrifugation (10,000 g, 30 min). The clarified supernatant was applied to HisTrap HP (5 ml; GE Healthcare) and pre-equilibrated with buffer A (50 mM HEPES, pH 8.0, 300 mM NaCl) using a peristaltic pump. The following steps were performed using an ÄKTA™ start System (GE Healthcare) equilibrated with buffer A. The column was washed with 5% (v/v) of elution buffer B (buffer A containing 500 mM imidazole). For elution of hSMUG1(25–270)-(His)×6-tag, the 25–500 mM imidazole gradient of buffer B was applied to the column for 30 min with a fractionation speed of 1 ml/min. Fractions containing hSMUG1(25–270)-(His)×6-tag were pooled, supplemented with 50 µl of AcTEV protease (Thermo Fisher Scientific) in dialysis buffer (50 mM HEPES, 300 mM NaCl, 2 mM 2-mercaptoethanol) and incubated overnight. After the TEV protease treatment, the protein solution was applied to a HiTrap Talon 1 ml column (GE Healthcare) equilibrated with buffer A using Äkta™ start System. The untagged hSMUG1(25–270) was collected in the flow-through using a fraction size of 1 ml. The hSMUG1(25–270) was analysed with SDS-PAGE. The pure fractions were concentrated using Vivaspin 6 with molecular weight cut-off (MWCO) of 10,000 Da (Sartorius Stedim Biotech). The concentration was measured using the Pierce™ BCA Protein Assay Kit (Thermo Fisher Scientific) and the protein was stored at -20 °C in 50% (v/v) glycerol. The band from the SDS-PAGE gel was analysed by MS that verified hSMUG1.

Table S1. MS analysis of commercial hSMUG1 preparation

Checked	Master	Accession	Description	Coverage	# Peptides	# PSMs	# Unique Peptides	# Protein Groups	# AAs	MW [kDa]	calc. pI	Protein FDR Confidence Mascot	Exp. q-value Mascot	Score Mascot	# Peptides Mascot
USANN	Master Protein	P02769	Serum albumin OS=Bos taurus GN=ALB PE=1 SV=4	77,59472817	57	589	42	1	607	69,248	6,18	High	0	17160,79704	57
USANN	Master Protein	P08835	Serum albumin OS=Sus scrofa GN=ALB PE=1 SV=2	17,6276771	13	123	1	1	607	69,647	6,49	High	0	2879,437004	13
USANN	Master Protein	P49822	Serum albumin OS=Canis lupus familiaris GN=ALB PE=1 SV=3	11,34868421	9	98	1	1	608	68,56	5,69	High	0	2348,265297	9
USANN	Master Protein	P02768	Serum albumin OS=Homo sapiens GN=ALB PE=1 SV=2	9,688013136	7	77	2	1	609	69,321	6,28	High	0	1658,559994	7
USANN	Master Protein	Q53HV7	Single-strand selective monofunctional uracil DNA glycosylase OS=Homo sapiens GN=SMUG1 PE=1 SV=2	59,25925926	13	55	9	1	270	29,842	6,62	High	0	1485,567343	13
USANN	Master Protein	P04264	Keratin, type II cytoskeletal 1 OS=Homo sapiens GN=KRT1 PE=1 SV=6	29,34782609	14	28	12	1	644	65,999	8,12	High	0	1056,903975	14
USANN	Master Protein	P00761	Trypsin OS=Sus scrofa PE=1 SV=1	25,10822511	4	28	4	1	231	24,394	7,18	High	0	736,6334541	4
USANN	Master Protein	P13645	Keratin, type I cytoskeletal 10 OS=Homo sapiens GN=KRT10 PE=1 SV=6	35,2739726	16	23	13	1	584	58,792	5,21	High	0	645,6170418	16
USANN	Master Protein	P49065	Serum albumin OS=Oryctolagus cuniculus GN=ALB PE=1 SV=2	10,36184211	8	22	2	1	608	68,865	6,24	High	0	501,912621	8
USANN	Master Protein	P35908	Keratin, type II cytoskeletal 2 epidermal OS=Homo sapiens GN=KRT2 PE=1 SV=2	31,14241002	14	17	9	1	639	65,393	8	High	0	437,6774163	14
USANN	Master Protein	P02538	Keratin, type II cytoskeletal 6A OS=Homo sapiens GN=KRT6A PE=1 SV=3	29,96453901	16	16	3	1	564	60,008	8	High	0	417,460209	16
USANN	Master Protein	P35527	Keratin, type I cytoskeletal 9 OS=Homo sapiens GN=KRT9 PE=1 SV=3	30,33707865	12	13	11	1	623	62,027	5,24	High	0	412,2821524	12
USANN	Master Protein	P04259	Keratin, type II cytoskeletal 6B OS=Homo sapiens GN=KRT6B PE=1 SV=5	25,35460993	14	15	1	1	564	60,03	8	High	0	356,1471413	14
USANN	Master Protein	Q6P5C5	Single-strand selective monofunctional uracil DNA glycosylase OS=Mus musculus GN=Smug1 PE=1 SV=1	20,43010753	5	16	1	1	279	30,635	6,77	High	0	355,1021782	5
USANN	Master Protein	P08779	Keratin, type I cytoskeletal 16 OS=Homo sapiens GN=KRT16 PE=1 SV=4	22,62156448	10	13	4	1	473	51,236	5,05	High	0	283,5066545	10
USANN	Master Protein	Q3SZR3	Alpha-1-acid glycoprotein OS=Bos taurus GN=ORM1 PE=2 SV=1	31,68316832	7	9	7	1	202	23,168	5,87	High	0	262,9563804	7
USANN	Master Protein	P02533	Keratin, type I cytoskeletal 14 OS=Homo sapiens GN=KRT14 PE=1 SV=4	23,51694915	10	13	3	1	472	51,529	5,16	High	0	252,2528084	10
USANN	Master Protein	A5A6M8	Keratin, type II cytoskeletal 5 OS=Pan troglodytes GN=KRT5 PE=2 SV=1	15,87837838	10	10	5	1	592	62,5	7,3	High	0	173,1344831	10
USANN	Master Protein	Q04695	Keratin, type I cytoskeletal 17 OS=Homo sapiens GN=KRT17 PE=1 SV=2	18,51851852	7	9	3	1	432	48,076	5,02	High	0	163,0714326	7
USANN	Master Protein	Q2UVX4	Complement C3 OS=Bos taurus GN=C3 PE=1 SV=2	2,046959663	3	3	3	1	1661	187,135	6,84	High	0	120,7966667	3
USANN	Master Protein	P41361	Antithrombin-III OS=Bos taurus GN=SERPINC1 PE=1 SV=2	4,946236559	2	3	2	1	465	52,314	7,33	High	0	82,02	2
USANN	Master Protein	P01030	Complement C4 (Fragments) OS=Bos taurus GN=C4 PE=1 SV=2	2,608695652	2	2	2	1	920	101,817	6,58	High	0	73,82	2
USANN	Master Protein	P50448	Factor XIIa inhibitor OS=Bos taurus PE=1 SV=1	2,564102564	1	1	1	1	468	51,691	6,67	High	0	70,76	1

LEGEND TO FIGURES

Figure S1. Conversion of UIP to 3′-OH product by hAPE1. Substrate 1[^{32}P] (0.12 pmol) was incubated at 37 °C alone (lane 1), with EcUng (0.78 pmol) and hOGG1 (13 pmol) for 10 min (lane 2), with hSMUG1 (0.3 pmol) for 10 min (lane 3) or with hSMUG1 (0.3 pmol) for 30 min followed by purification of DNA on a column and incubation with hAPE1 (0.45 pmol) for 10 min (lane 4). Denaturing PAGE was performed on a 20% (w/v) minigel.

Figure S2. SDS-PAGE of purified hSMUG(25–270). Lane 2, fraction pool (4 µg) from the first HisTrap (5 ml) affinity chromatography step, which was treated with TEV protease and dialysed; lanes 3 and 4, fractions 3 and 5 (2 µg each), respectively, from the second HiTrap Talon crude (1 ml) affinity chromatography step to separate hSMUG(25–270) from His-tagged enzyme and TEV protease. The molecular weight marker (MWM; lane 1) is Precision Plus Protein™ Unstained Protein Standards (10 µl), Strep-tagged recombinant, from BioRad (product #1610363).

Figure S3. MALDI-TOF-MS signals for control incubation of U-DNA without enzyme. The lack of the MALDI-TOF-MS signal corresponding to UIP and UPP is indicated by comparing the analysis presented here with the analyses described in Figure 8A. Substrate (unlabelled substrate 2; Figure 8A) alone was incubated in 20 mM Tris-HCl, pH 8.0, 1 mM DTT, 1 mM EDTA, 70 mM KCl at 37 °C for 1 h.

Figure S4. MALDI-TOF-MS signals for incubation of U-DNA with hSMUG1 with and without hAPE1. hSMUG1 (0.3 pmol) was incubated with unlabelled substrate 2 (100 pmol) in 20 mM Tris-HCl, pH 8.0, 1 mM DTT, 1 mM EDTA, 70 mM KCl at 37 °C for 10 min, followed by incubation with (upper graph) and without (lower graph) hAPE1 (0.45 pmol) for 2 h. Following precipitation twice (before and after hAPE1 addition, in the presence of sodium acetate and ammonium acetate, respectively; see Materials and Methods), the DNA was dissolved in 10 µl water for MS analysis (200 ng/µl).

Figure S5. U-DNA incision rate of hSMUG1 (V^{in}; see Figure 9A) as a function of enzyme concentration $[E]_0$ at an initial U-DNA concentration $[S]_0$ of (**A**) 125 nM or (**B**) 375 nM, where incubation was performed for 20 min as described in Figure 4B. Each value represents the average (± SD) of 3–6 independent measurements.

REFERENCES

1. Asagoshi, K., Yamada, T., Terato, H., Ohyama, Y., Monden, Y., Arai, T., Nishimura, S., Aburatani, H., Lindahl, T. and Ide, H. (2000) Distinct repair activities of human 7,8-dihydro-8-oxoguanine DNA glycosylase and formamidopyrimidine DNA glycosylase for formamidopyrimidine and 7,8-dihydro-8-oxoguanine. *J Biol Chem*, **275**, 4956–4964.
2. Radicella, J.P., Dherin, C., Desmaze, C., Fox, M.S. and Boiteux, S. (1997) Cloning and characterization of *hOGG1*, a human homolog of the *OGG1* gene of *Saccharomyces cerevisiae*. *Proc Natl Acad Sci USA*, **94**, 8010–8015.
3. Bailly, V. and Verly, W.G. (1987) *Escherichia coli* endonuclease III is not an endonuclease but a β-elimination catalyst. *Biochem J*, **242**, 565–572.
4. Mazumder, A., Gerlt, J.A., Absalon, M.J., Stubbe, J., Cunningham, R.P., Withka, J. and Bolton, P.H. (1991) Stereochemical studies of the *β*-elimination reactions at aldehydic abasic sites in DNA: endonuclease III from *Escherichia coli*, sodium hydroxide, and Lys-Trp-Lys. *Biochemistry*, **30**, 1119–1126.
5. Piersen, C.E., McCullough, A.K. and Lloyd, R.S. (2000) AP lyases and dRPases: commonality of mechanism. *Mutat Res*, **459**, 43–53.
6. McCullough, A.K., Sanchez, A., Dodson, M.L., Marapaka, P., Taylor, J.S. and Lloyd, R.S. (2001) The reaction mechanism of DNA glycosylase/AP lyases at abasic sites. *Biochemistry*, **40**, 561–568.
7. Fromme, J.C. and Verdine, G.L. (2003) Structure of a trapped endonuclease III-DNA covalent intermediate. *EMBO J*, **22**, 3461–3471.
8. Bjørås, M., Luna, L., Johnsen, B., Hoff, E., Haug, T., Rognes, T. and Seeberg, E. (1997) Opposite base-dependent reactions of a human base excision repair enzyme on DNA containing 7,8-dihydro-8-oxoguanine and abasic sites. *EMBO J*, **16**, 6314–6322.
9. Sun, B., Latham, K.A., Dodson, M.L. and Lloyd, R.S. (1995) Studies on the catalytic mechanism of five DNA glycosylases. Probing for enzyme-DNA imino intermediates. *J Biol Chem*, **270**, 19501–19508.
10. Chung, S.J. and Verdine, G.L. (2004) Structures of end products resulting from lesion processing by a DNA glycosylase/lyase. *Chem Biol*, **11**, 1643–1649.
11. Darwanto, A., Farrel, A., Rogstad, D.K. and Sowers, L.C. (2009) Characterization of DNA glycosylase activity by matrix-assisted laser desorption/ionization time-of-flight mass spectrometry. *Anal Biochem*, **394**, 13–23.
12. Castellan, G.W. (1983) *Physical Chemistry*. 3 ed. Addison-Wesley, Reading, Massachusetts.

Figure S1

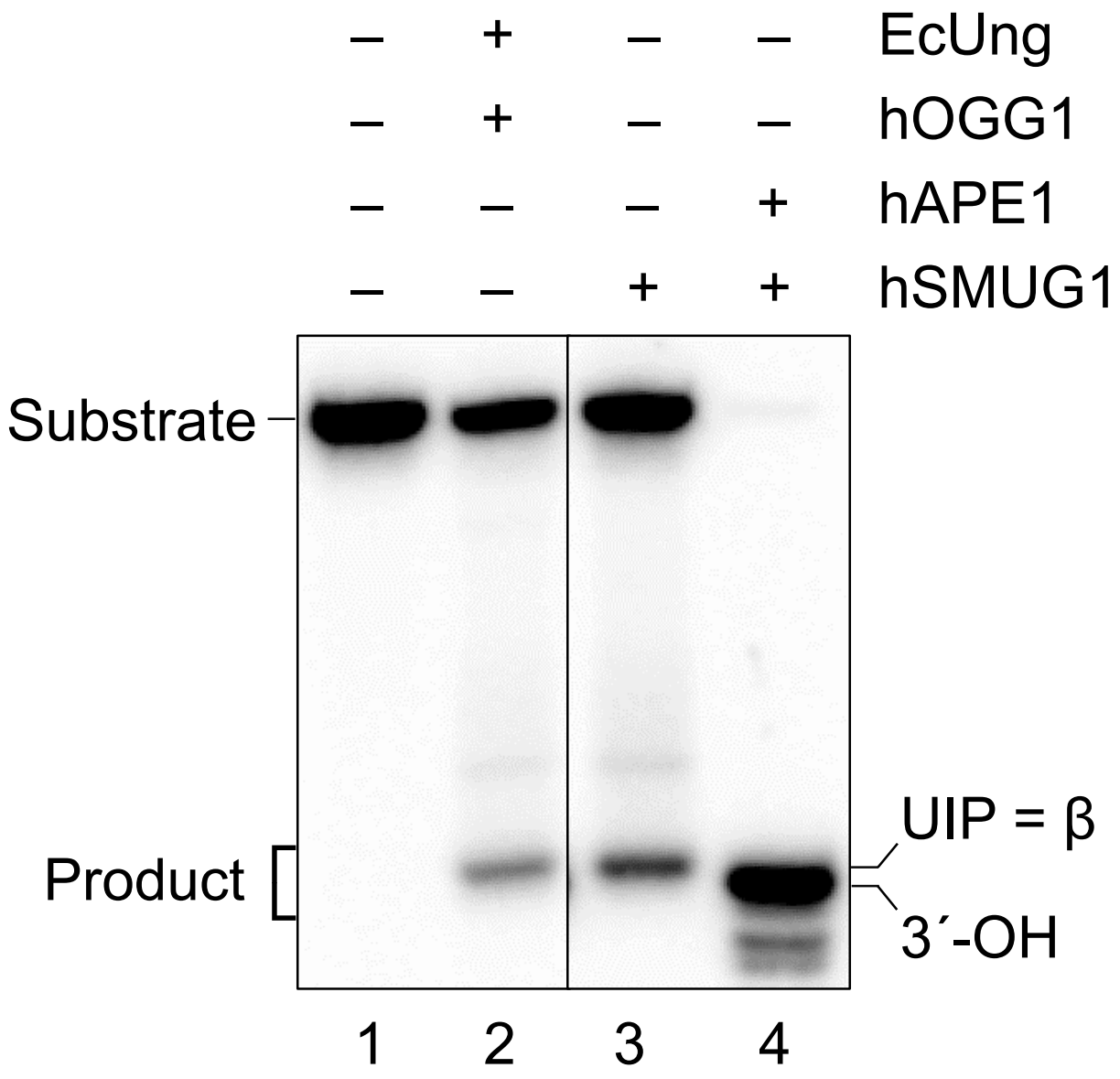

Figure S2

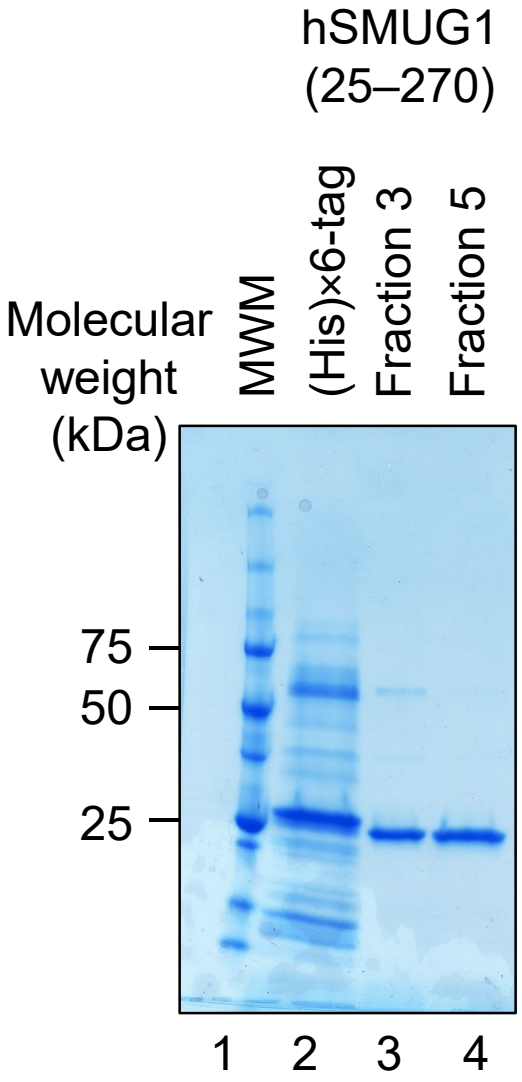
hSMUG1
(25–270)
Molecular
weight
(kDa)
MWM
(His)×6-tag
Fraction 3
Fraction 5
75
50
25
1
2
3
4

Figure S3

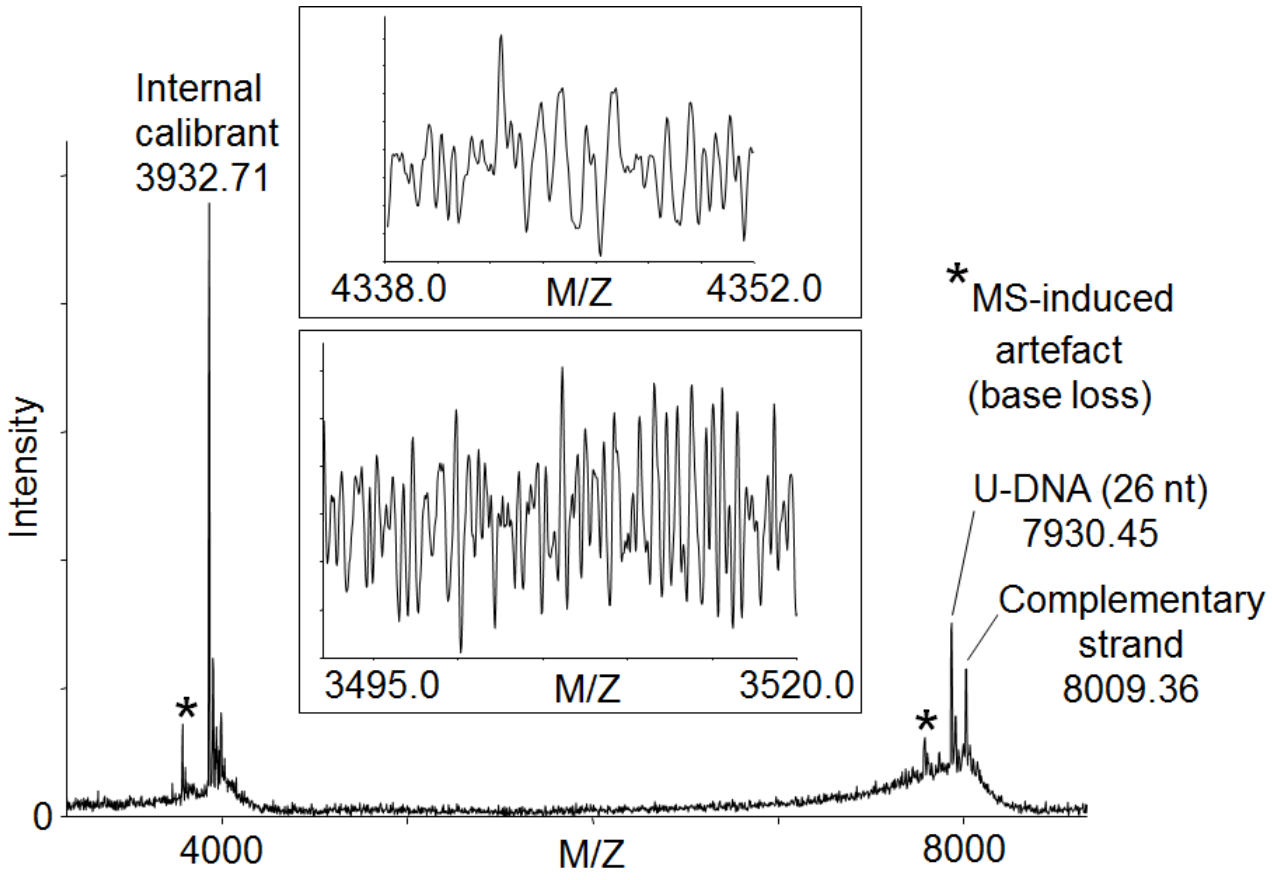
Internal
calibrant
3932.71
4338.0
M/Z
4352.0
3495.0
M/Z
3520.0
*MS-induced
artefact
(base loss)
U-DNA (26 nt)
7930.45
Complementary
strand
8009.36
Intensity
0
4000
M/Z
8000

Figure S4

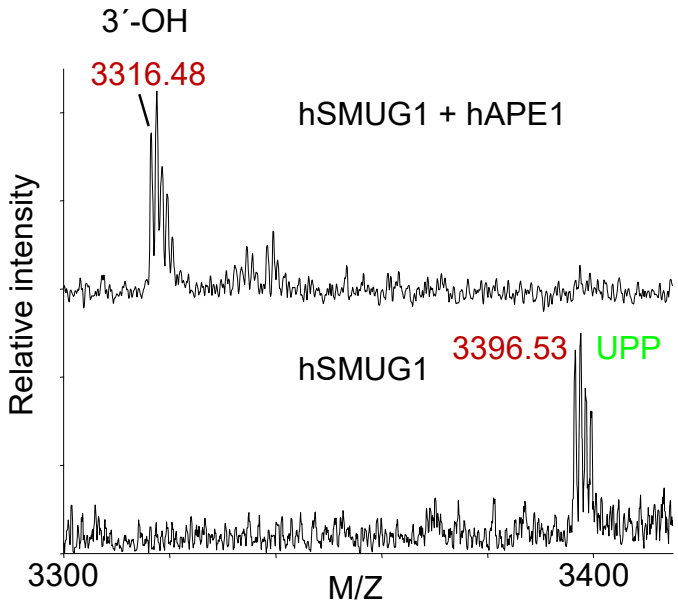
3´-OH
3316.48
hSMUG1 + hAPE1
Relative intensity
hSMUG1
3396.53
UPP
3300
M/Z
3400

Figure S5

A

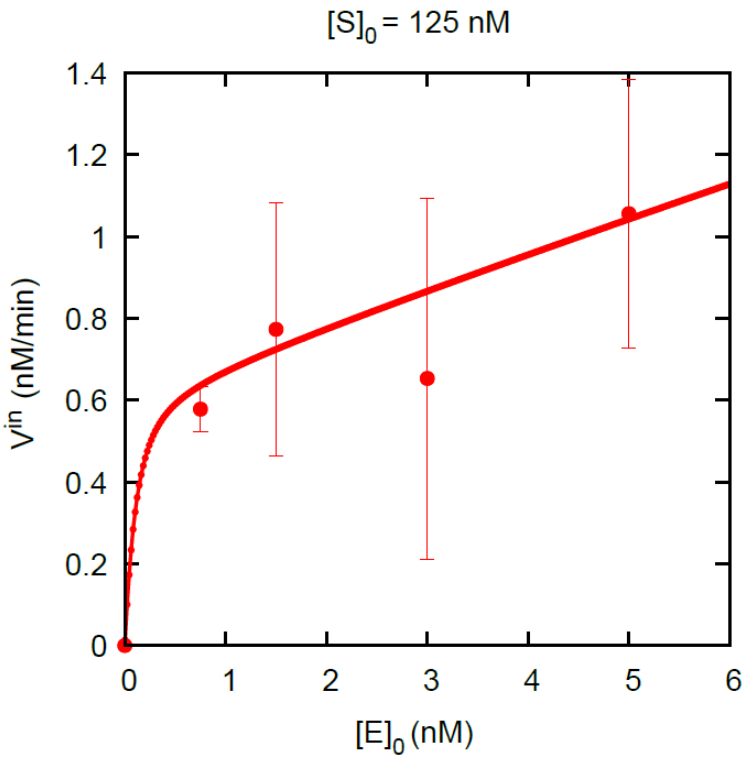
[S]0 = 125 nM
1.4
1.2
1
0.8
0.6
0.4
0.2
0
Vin (nM/min)
0
1
2
3
4
5
6
[E]0 (nM)

B

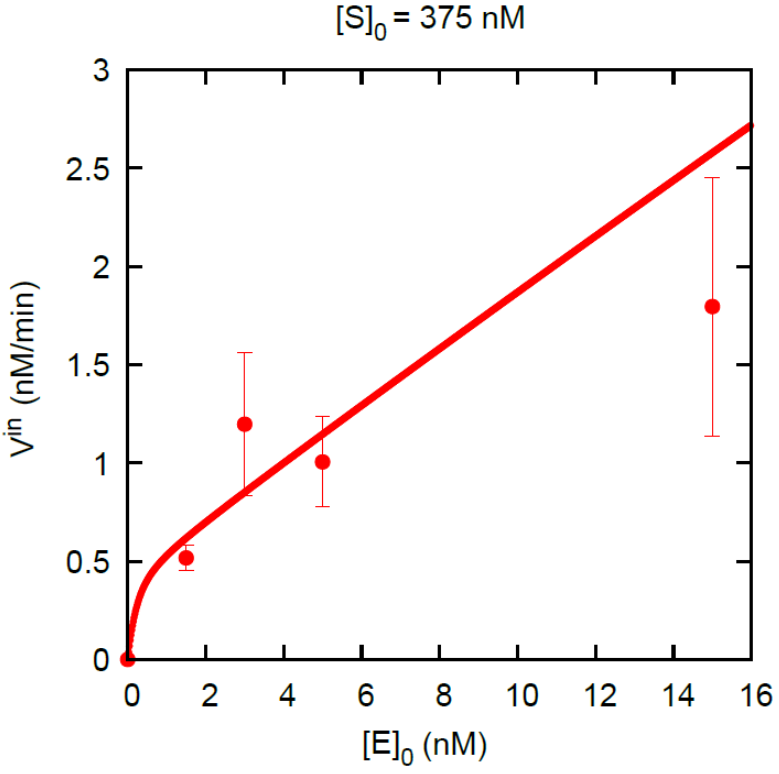
[S]0 = 375 nM
3
2.5
2
1.5
1
0.5
0
Vin (nM/min)
0
2
4
6
8
10
12
14
16
[E]0 (nM)